Preparation, Crystal Structure, and Magnetic and Magnetotransport Properties of the Double Perovskite Ca_2FeMoO_6

J. A. Alonso,*,† M. T. Casais,† M. J. Martínez-Lope,† J. L. Martínez,† P. Velasco,† A. Muñoz,‡ and M. T. Fernández-Díaz§

Instituto de Ciencia de Materiales de Madrid, C.S.I.C., Cantoblanco, E-28049 Madrid, Spain, Depto. de Física, EPS, University Carlos III, Butarque 15, Leganés, E-28911 Madrid, Spain, and Institut Laue-Langevin, B.P. 156, F-38042 Grenoble Cedex 9, France

Received August 9, 1999

Ca_2FeMoO_6 perovskite has been prepared in polycrystalline form by controlled reduction of previously decomposed citrate precursors. This material has been studied by X-ray and neutron powder diffraction (NPD), scanning electron microscopy, thermal analysis, and magnetic and magnetotransport measurements. The crystal structure is monoclinic, space group $P2_1/n$, with $a = 5.4150(1)$, $b = 5.5224(1)$, $c = 7.7066(2)$ Å, and $\beta = 89.969(8)°$ at room temperature (RT). The crystal contains alternating FeO_6 and MoO_6 octahedra, considerably tilted due to the relatively small size of the Ca^{2+} cations. Low-temperature (2 K) NPD data show evidence for a ferrimagnetic coupling between the Fe^{3+} and Mo^{5+} sublattices, with ordered magnetic moments of 3.2(1) and −0.76(6) μ_B, respectively. The Curie temperature is 380 K. Both magnetism and transport indicate a large component of itinerancy for down-spin Fe t_{2g} electrons. The carrier density measured by the Hall effect is 0.031 holes per formula unit at 100 K. A magnetoresistance of 30% has been observed at RT for 9*T*, significantly larger than that reported for other A_2FeMoO_6 perovskites, A = Sr, Ba.

Introduction

Materials exhibiting colossal magnetoresistance (CMR) undergo a large change in electrical resistance in response to an external magnetic field. This effect is of technological interest, as it can be exploited for the detection of magnetic fields in magnetic memory devices. A range of compounds have now been found to exhibit intrinsic CMR;[1,2] most of them are manganese perovskites based on $LaMnO_3$. Hole doping of this insulating compound produces Mn^{4+} cations and thus creates itinerant e_g holes, which can hibridize with the O(2p) state. A double-exchange interaction between Mn^{3+} and Mn^{4+} mediates ferromagnetic interaction, and the material exhibits metallic conduction below the Curie temperature (T_C). Near T_C an external magnetic field tends to align the local spins, and then electron transfer increases, resulting in the observed decrease in resistivity. In addition, lattice anomalies associated with changes in spin alignment and/or electron transfer are often observed, suggesting a correlation between spin and lattice.[3−5] Static and/or dynamic Jahn−Teller distortions of the MnO_6 octahedra are also suspected to play an important role in the observed behavior.[6]

Recently, some members of the family of double perovskites of composition $A_2B'B''O_6$ (A = alkali earths, B′, B″ = transition metals) have been proposed as half-metallic ferromagnets, as an alternative to perovskite manganites.[7−11] At first, Sr_2FeMoO_6 was shown to exhibit intrinsic tunneling-type magnetoresistance at room temperature (RT).[7,11] In this material the B positions of the perovskite structure are occupied alternately by Fe and Mo atoms, in such a way that each FeO_6 octahedron is corner-linked to six MoO_6 octahedra and vice-versa. Sr_2FeMoO_6 is well-known[12,13] to be a ferromagnet (or ferrimagnet) below a characteristic Curie temperature (T_C) of 410−450 K. The magnetic structure was described[7] as an ordered arrangement of parallel Fe^{3+} ($3d^5$, $S = 5/2$) magnetic moments, antifer-

* To whom correspondence should be addressed.
† Instituto de Ciencia de Materiales de Madrid.
‡ University Carlos III.
§ Institut Laue-Langevin.

(1) Ramirez, A. P. *J. Phys.: Condens. Matter* **1997,** *9*, 8171.
(2) Rao, C. N. R., Raveau, B., Eds. Colossal magnetoresistance and other *related properties in 3d oxides*; World Scientific: Singapore, **1998**.
(3) Radaelli, P. G.; Cox, D. E.; Marezio, M.; Cheong, S.-W.; Schiffer, P. E.; Ramirez, A. P. *Phys. Rev. Lett.* **1995**, *75*, 4488.
(4) Röder, H.; Hang, J.; Bishop, A. R. *Phys. Rev. Lett.* **1996**, *76*, 1356.
(5) De Teresa, J. M.; Ibarra, M. R.; Algarabel, P. A.; Ritter, C.; Marquina, C.; Blasco, J.; García, J.; del Moral, A.; Arnold, Z. *Nature* **1997**, *386*, 256.
(6) Millis, A. J.; Shraiman, B. I.; Mueller, R. *Phys. Rev. Lett.* **1996**, *77*, 175.
(7) Kobayashi, K.-I.; Kimura, T.; Sawada, H.; Terakura, K.; Tokura, Y. *Nature* **1998**, *395*, 677.
(8) García-Landa, B.; Ritter, C.; Ibarra, M. R.; Blasco, J.; Algarabel, P. A.; Mahendiran, R.; García, J. *Solid State Commun.* **1999**, *110*, 435.
(9) Maignan, A.; Raveau, B.; Martin, C.; Hervieu, M. *J. Solid State Chem.* **1999**, *144*, 224.
(10) Kobayashi, K.-I.; Kimura, T.; Tomioka, Y.; Sawada, H.; Terakura, K.; Tokura, Y. *Phys. Rev. B* **1999**, *59*, 11159.
(11) Kim, T. H.; Uehara, M.; Cheong, S.-W.; Lee, S. *Appl. Phys. Lett.* **1999**, *74*, 1737.
(12) Patterson, F. K.; Moeller, C. W.; Ward, R. *Inorg. Chem.* **1963**, *2*, 196.
(13) Galasso, F.; Douglas, F.; Kasper, R. J. *Chem. Phys.* **1966**, *44*, 1672.

10.1021/cm990512g CCC: $19.00
Published on Web 12/11/1999

romagnetically coupled with Mo^{5+} ($4d^1$, $S = {}^1/_2$) spins. The observed MR has been associated with electron tunneling through the insulator barrier formed by the grain boundaries. Later on, neutron diffraction studies on this material[8] seemed to discard the existence of a ferrimagnetic state below T_C, rather suggesting the electronic configuration $Fe^{2+}Mo^{6+}$ instead of $Fe^{3+}Mo^{5+}$, consistent with the ordered magnetic moment observed for Fe of 4.0 μ_B. These results support the itinerant character of the t_{2g} Mo electron, giving no local magnetic moment at the Mo sites.

Further studies on other members of the $A_2B'B''O_6$ family seem to indicate that the occurrence of MR properties is a common feature in some of them. Thus, large intragrain (bulk) MR above RT has been described in the double perovskite Ba_2FeMoO_6, also exhibiting metallic and ferrimagnetic ($T_C = 340$ K) properties.[9] As well, Sr_2FeReO_6 ($T_C = 415$ K) presents[10] a half metallic ground state, concomitant with the ferrimagnetic coupling of Fe^{3+} and Re^{5+} ($5d^2$, $S = {}^2/_2$) magnetic moments, and shows significant intergrain tunneling MR at RT. These results encourage us to explore other prospective half metallic compounds as MR materials with sufficiently large effect at low magnetic fields, in ferromagnetic compounds with T_C's as close as possible to RT.

We focused our attention on the Ca analogue of the A_2FeMoO_6 family. Ca_2FeMoO_6 perovskite was first studied a long time ago.[12,14] A Curie temperature of $T_C = 377$ K was reported for this material, and its structure was described as an orthorhombic distortion of perovskite,[12] with unit-cell parameters $a = 5.53$, $b = 7.73$, and $c = 5.42$ Å. This is in contrast with the cubic symmetry found for both Sr_2FeMoO_6[8] and Ba_2FeMoO_6.[9] The lowering of symmetry described for the Ca analogue is a consequence of the reduction of the tolerance factor of the perovskite structure, $t = d_{A-O}/\sqrt{2}d_{B-O}$, as the A^{2+} size decreases from Sr^{2+} to Ca^{2+}. In the present work we describe the synthesis of this material, which must be prepared in controlled reducing conditions, and the results of a neutron powder diffraction (NPD) study on a well-crystallized Ca_2FeMoO_6 sample. The structure has been revisited: we report complete structural data for this monoclinically distorted perovskite, which contains two crystallographically independent sites for Fe and Mo cations. Low-temperature NPD data allowed us to probe the microscopic origin of the magnetic ordering, concerning both Fe^{3+} and Mo^{5+} magnetic moments. The magnetic and magnetotransport properties are also discussed in the light of the NPD data.

Experimental Section

Ca_2FeMoO_6 was prepared as a black pollycrystalline powder from stoichiometric amounts of analytical grade $CaCO_3$, $C_2O_4Fe{\cdot}2H_2O$, and $(NH_4)_2Mo_7O_{24}$, which were solved in citric acid, by adding several droplets of concentrated HNO_3. The citrate + nitrate solution was slowly evaporated, leading to an organic resin containing a random distribution of the involved cations at an atomic level. The resin was first dried at 120 °C, leading to a very porous and voluminous "sponge-cake-like" material, which was ground and slowly decomposed at temperatures up to 600 °C. The sample was then heated at 800 °C for 2 h in order to eliminate all the organic materials and nitrates. This treatment gave rise to a highly reactive precursor material, which was heated under an reducing $H_2(5\%)/N_2$ flow at 400 °C h^{-1} up to 850 °C; then the sample was immediately left to slowly cool to RT in the reaction vessel. It is worth mentioning that longer treatments at 850 °C invariably lead to reduction products of Fe or Mo oxides.

The product was initially characterized by laboratory XRD (Cu Kα, $\lambda = 1.5406$ Å) for phase identification and to assess phase purity. For the structural refinements, NPD patterns of Ca_2FeMoO_6 were collected at room temperature and 2 K at the high-resolution D2B neutron diffractometer of ILL-Grenoble. The high-flux mode was used. About 4 g of sample were contained in a vanadium can; a collecting time of 3 h was required for each pattern. A wavelength of 1.594 Å was selected from a Ge monochromator. High-temperature medium-resolution NPD patterns were collected at the D1B diffractometer, to follow the thermal evolution of the ferromagnetic component. The sample was placed in a vanadium furnace and heated under vacuum conditions. The collecting temperatures were 290, 350, 400, 500, 600, 850, and 900 K. All the patterns were refined by the Rietveld method, using the FULLPROF refinement program.[15] A pseudo-Voigt function was chosen to generate the line shape of the diffraction peaks. No regions were excluded in the refinement. In the final run the following parameters were refined from the D2B data: scale factor, background coefficients, zero-point error, unit-cell parameters, pseudo-Voigt corrected for asymmetry parameters, positional coordinates, isotropic thermal factors, and magnitudes of the Mo and Fe magnetic moments. The coherent scattering lengths for Ca, Fe, Mo, and O were 4.70, 9.45, 6.72, and 5.803 fm, respectively. The magnetic form factors considered for Fe and Mo cations were determined with the coefficients taken from the International Tables.

Scanning electron microscopy (SEM) micrographs were taken in a Philips XL30 microscope at an accelerating voltage of 15 kV and magnification values up to 20 000×. The Ca_2FeMoO_6 SEM images were taken on compacted pellets, sintered under the same synthetic conditions (temperature, atmosphere) as the raw powder. Thermal analysis was carried out in a Mettler TA3000 system equipped with a TC10 processor unit. Thermogravimetric (TG) curves were obtained in a TG50 unit, working at a heating rate of 5 °C min^{-1}, in an air flow of 0.3 l min^{-1}. About 50 mg of sample was used in the experiment. The dc and ac magnetic susceptibilities were measured with a commercial SQUID magnetometer on powdered samples, in the temperature range 1.5−850 K; transport and magnetotransport measurements were performed by the conventional four-probe technique, under magnetic fields up to 9 T in a PPMS system from Quantum Design, in sintered pellets of $10 \times 3 \times 2$ mm^3.

Results

Ca_2FeMoO_6 was obtained as a black, well-crystallized powder. The laboratory XRD diagram is shown in Figure 1. The pattern is characteristic of a strongly distorted perovskite showing sharp, well-defined superstructure reflections. No impurity phases were detected from either XRD or NPD data. A micrograph picture (Figure 2) of as-grown Ca_2FeMoO_6 illustrates the high homogeneity of this material. Figure 2 shows the presence of porosity, probably formed during the elimination of organic materials. Ca_2FeMoO_6 microcrystals are distributed around the pores. It also shows the shape and size of Ca_2FeMoO_6 microcrystals, in the range 0.3−0.5 μm large. A good sintering between neighbor grains is observed.

Thermal Analysis. The sample is stable in air up to 380 °C; above this temperature an oxidation process

(14) Galasso, F. *Structure, Properties and Preparation of Perovskite-Type Compounds*; Pergamon Press: Oxford, 1969.

(15) Rodríguez-Carvajal, J. *Physica B (Amsterdam)* **1993**, *192*, 55.

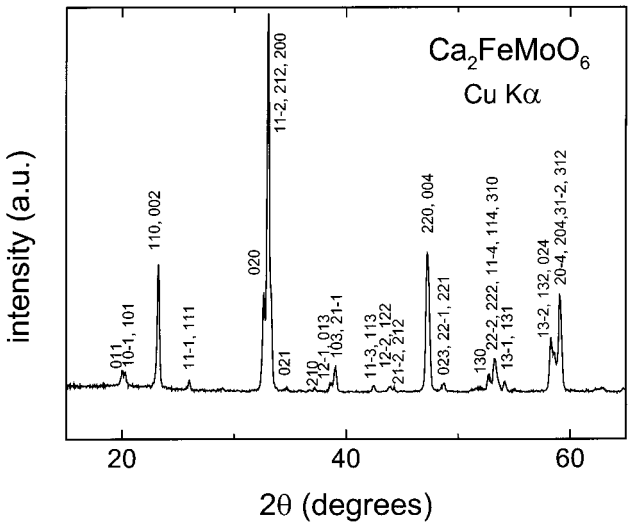

Figure 1. XRD pattern for Ca_2FeMoO_6, indexed in a monoclinic unit cell with $a \approx \sqrt{2}a_0$, $b \approx \sqrt{2}a_0$, $c \approx 2a_0$, $\beta \approx 90°$, and $a_0 \approx 3.8$ Å.

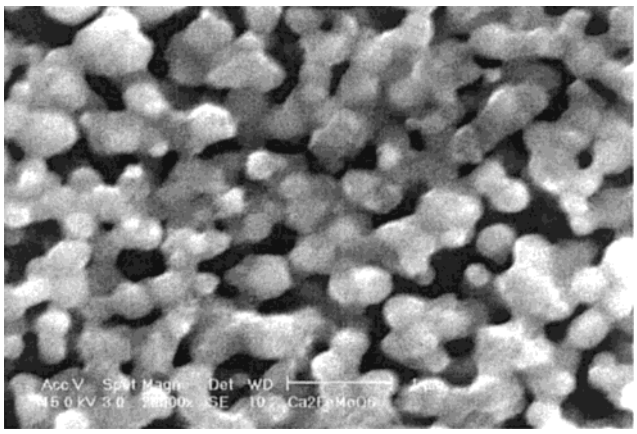

Figure 2. Scanning electron micrograph of a sintered pellet of Ca_2FeMoO_6, taken at a magnification of 20 000×.

starts, leading to the complete decomposition of the perovskite. The weight gain corresponds to the incorporation of $^1/_4O_2$ per perovskite formula, that is, to the complete oxidation of Mo^{5+} to Mo^{6+}. The product of the oxidation has been identified by XRD as a mixture of $CaMoO_4$ and $Ca_2Fe_2O_5$.

Magnetic Data. The magnetization versus temperature data (Figure 3a) show a low-temperature saturation for Ca_2FeMoO_6 characteristic of the spontaneous ferromagnetic ordering described earlier.[11] The magnetization versus magnetic field data shown in Figure 3b at 2 K are characteristic of a ferromagnet with a saturation magnetic moment of 2.5 μ_B per formula unit. At 290 K this material is still strongly ferromagnetic, showing a moment saturation of 1.1 μ_B/f.u. The inflection in the magnetization at 380 K, labeled as T_C in Figure 3a, is close to the reported Curie temperature for this material, of 377 K.[12] However, our high-temperature measurements show an additional inflection at above 700 K (better appreciated in the reciprocal susceptibility curve), corresponding to the onset of a weak ferromagnetism effect which had not been described before. Although the data were recorded up to 780 K, by extrapolating the temperature at which the magnetization cancels, we estimate the onset of this weak effect at ~795 K. Figure 3b gives evidence for the

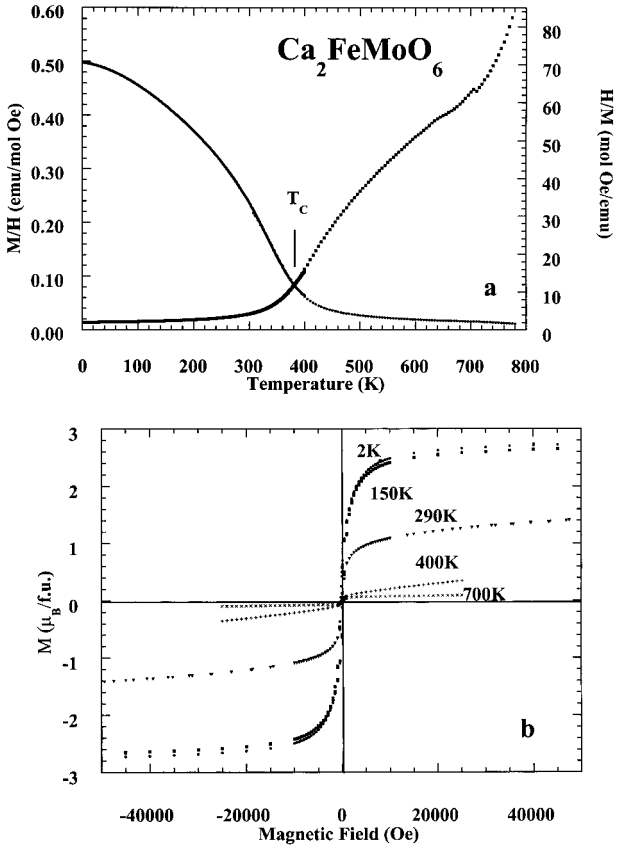

Figure 3. (a) Temperature dependence of the dc magnetic susceptibility and reciprocal susceptibility. (b) Magnetization versus field isotherms for selected temperatures.

existence of a ferromagnetic state at 700 K, with a small but significant saturation moment of 0.07 μ_B. No Curie–Weiss behavior was observed in the measured temperature range from the reciprocal susceptibility data (Figure 3a). This second anomaly could be intrinsic, but due to the small moment and the high temperature involved, we are tempted to assign it to a small impurity of Fe_3O_4 or Fe metal (or an FeMo alloy), produced during the reduction process in $H_2(5\%)/N_2$. This ferromagnetic impurity would be present as small (probably amorphous) particles which could not be detected by diffraction methods.

Structural Refinement. The structural refinement from RT, high-resolution NPD data was first performed in the conventional *Pbnm* orthorhombic model, with unit-cell parameters related to a_0 (ideal cubic perovskite, $a_0 \approx 3.8$ Å) as $a \approx \sqrt{2}a_0$, $b \approx \sqrt{2}a_0$, and $c \approx 2a_0$, using the $GdFeO_3$ structure as a starting model, with Ca atoms at 4c (x, y, $^1/_4$) positions, Fe and Mo randomly distributed at 4b ($^1/_2$, 0, 0) positions, and O1 and O2 at 4c and 8d (x, y, z) sites of the *Pbnm* space group. The reasonable fit ($R_I \approx 8\%$) obtained for this preliminary model allowed us to confirm that the tilting scheme of the $(Fe,Mo)O_6$ octahedra corresponds to a $GdFeO_3$-like distortion of the perovskite. However, after this refinement, several superstructure reflections remained unexplained, arising from the ordering of Fe and Mo in the B sublattice of the perovskite. These reflections made it necessary to consider a lowering in the crystal symmetry with respect to the orthorhombic *Pbnm* model.

The structure was successfully refined in the monoclinic $P2_1/n$ space group, which is a subgroup of $Pbnm$. In $P2_1/n$ it is necessary to define two crystallographically independent B positions (Fe and Mo), as well as 3 kinds of nonequivalent oxygen atoms (O1, O2, and O3), all in general (x, y, z) positions. The refinements in the monoclinic model showed a significant improvement in reliability factor: R_I dropped to 5.5%. The monoclinic β angle is only slightly different from 90°, ~89.97°: the metric of this structure seems to be strongly pseudo-orthorhombic.

Magnetic Structure. The 2K NPD data reveal a strong magnetic contribution to the low-angle reflections, especially visible at the [011] Bragg position, at ~20.5° (see Figure 4). A ferromagnetic structure was modeled with magnetic moments at the Fe positions; after the full refinement of the profile, including the magnetic moment magnitude and orientation, a discrepancy factor R_{mag} of ~8% was reached. The further introduction of magnetic moments at the Mo positions in an antiferromagnetic arrangement with respect to Fe moments lead to a dramatic improvement of the refinement: R_{mag} dropped to ~4% for the final parameters listed in Table 1. After the final refinement, ordered moments of 3.2(1) μ_B and −0.76(6) μ_B were obtained for the Fe and Mo positions, respectively. Trials to couple ferromagnetically Fe and Mo moments invariably led to a serious deterioration of the fit. The spatial orientation of the moments is affected by a large error of ±10°; the best refinement was obtained for the polar angles $\varphi \sim 54°$ and $\theta \sim 90°$. The magnetic structure can be described as a ferrimagnetic arrangement of Fe and Mo moments lying in the bc plane, approximately along the [110] direction.

The refinement of the RT, high-resolution data was completed after the introduction of the magnetic contribution arising from both Fe and Mo atoms, non-negligible at RT, as shown from the magnetic measurements (Figure 3a and b). The magnitudes of the ordered magnetic moments were 1.7(2) and 0.5(2) μ_B at the Fe and Mo positions, respectively. Table 1 includes the unit-cell, atomic, and thermal parameters and the discrepancy factors. Figure 4 shows the agreement between observed and calculated NPD profiles. Table 2 contains a list of selected bond distances and angles. The thermal evolution of the structure and magnetism above RT was studied from D1B NPD data. Figure 5 shows the unit-cell parameter variation up to 900 K. In a trial to find out the microscopic origin of the magnetization inflection observed at ~795 K, the refinement of the Fe and Mo magnetic moments was performed in the patterns collected below this temperature. However, the small magnitude and the large error bars of the involved magnetic moments made unreliable the results of such refinements.

Magnetotransport Measurements. The transport properties of Ca_2FeMoO_6 are illustrated in Figure 6. Both $\rho(H=0)$ and $\rho(H=9T)$ show a metallic behavior over the whole temperature range, down to 2 K. It is worth mentioning that the observed value for $\rho(T=300K,H=0)$, of 1.8×10^{-4} Ω cm is considerably smaller than that of the Sr and Ba analogues, of 8×10^{-3} and 2×10^{-3} Ω cm, respectively.[8,9] These high values probably indicate that the resistance of the Sr and Ba samples is dominated by the carrier scattering at the grain boundaries. Our Ca sample, characterized by a homogeneous particle size, probably presents a better connectivity, in such a way that the measurements provide a better approximation of the bulk (intragrain) resistivity. Despite the severe distortion of the Ca perovskite and the correspondingly lower degree of orbital overlapping, a good metallicity is observed for this material, suggesting an important electronic itinerancy. Regarding the changes in $\rho(T)$ under a magnetic field, we define MR-(9T) = 100[R(0) − R(9T)]/R(9T). The evolution of MR-(9T) is shown as an inset of Figure 6. Although the curve exhibits an important noise (due to the small values of the measured resistances), an overall increase of MR is observed as T increases. There is an specially abrupt increase of MR above 270 K. The comparison with the MR variation observed for Ba_2FeMoO_6 is interesting.[9] In the Ba compound two temperature ranges were distinguished: between 10 and 250 K a smooth decrease of MR was observed, characterized by an abrupt drop of MR at low field, attributed to grain boundary effects; from 280 to 350 an increase in MR was found, showing a maximum close to T_C (330 K), which was attributed to intrinsic (intragrain) effects. By contrast, in the Ca perovskite (inset of Figure 6), the MR versus T variation in the low-temperature regime (below 270 K) suggests that the grain-boundary effects are minor and that the predominant feature in the abrupt enhancement of MR at temperatures close to T_C is of intragranular nature. At RT, MR(9T) is about 30%. This is comparable to the best results obtained for perovskite manganites, with large cations at the A positions, showing MR in the 10^2% range. Although many published results correspond to MR(7T), the comparison with our MR(9T) is pertinent, since for such very-high-field values the magnetization has largely reached saturation, and therefore changes in both intrinsic and extrinsic (intergrain) MR from 7T to 9T can be evaluated in a few percents. Also, MR-(300K) is significantly higher than that observed for the Sr and Ba compounds: for A_2FeMoO_6, MR(300K,7T) = 10% for A = Sr[7] and MR(330K,7T) = 15% for A = Ba.[9] A large intergrain magnetoresistance in low field has also been reported for the Sr material, of 6% at 1.5T.[11] As commented before, the observed MR for our Ca sample probably stands for intrinsic (intragrain) magnetoresistance, given the small value of the absolute resistivity, suggesting a good connectivity between grains. Hall coefficient measurements performed on Ca_2FeMoO_6 as well as Sr_2FeMoO_6 give −0.046 cm^3 per Coulomb and −0.012 cm^3 per Coulomb, respectively. At 100 K the carriers involved in the conduction are holes (in both cases), and the number of charge carrier, per formula unit is 0.031 for Ca_2FeMoO_6 and 0.12 for Sr_2FeMoO_6.

Discussion

The structure of the monoclinically distorted Ca_2FeMoO_6 perovskite contains three inequivalent oxygen positions, which cannot be very accurately determined by XRD, as strong pseudosymmetry is present in the patterns. Probably for this reason, this material had previously been described as orthorhombic.[12] A NPD study was essential to investigate the subtle structural features of this perovskite, neutrons being more sensi-

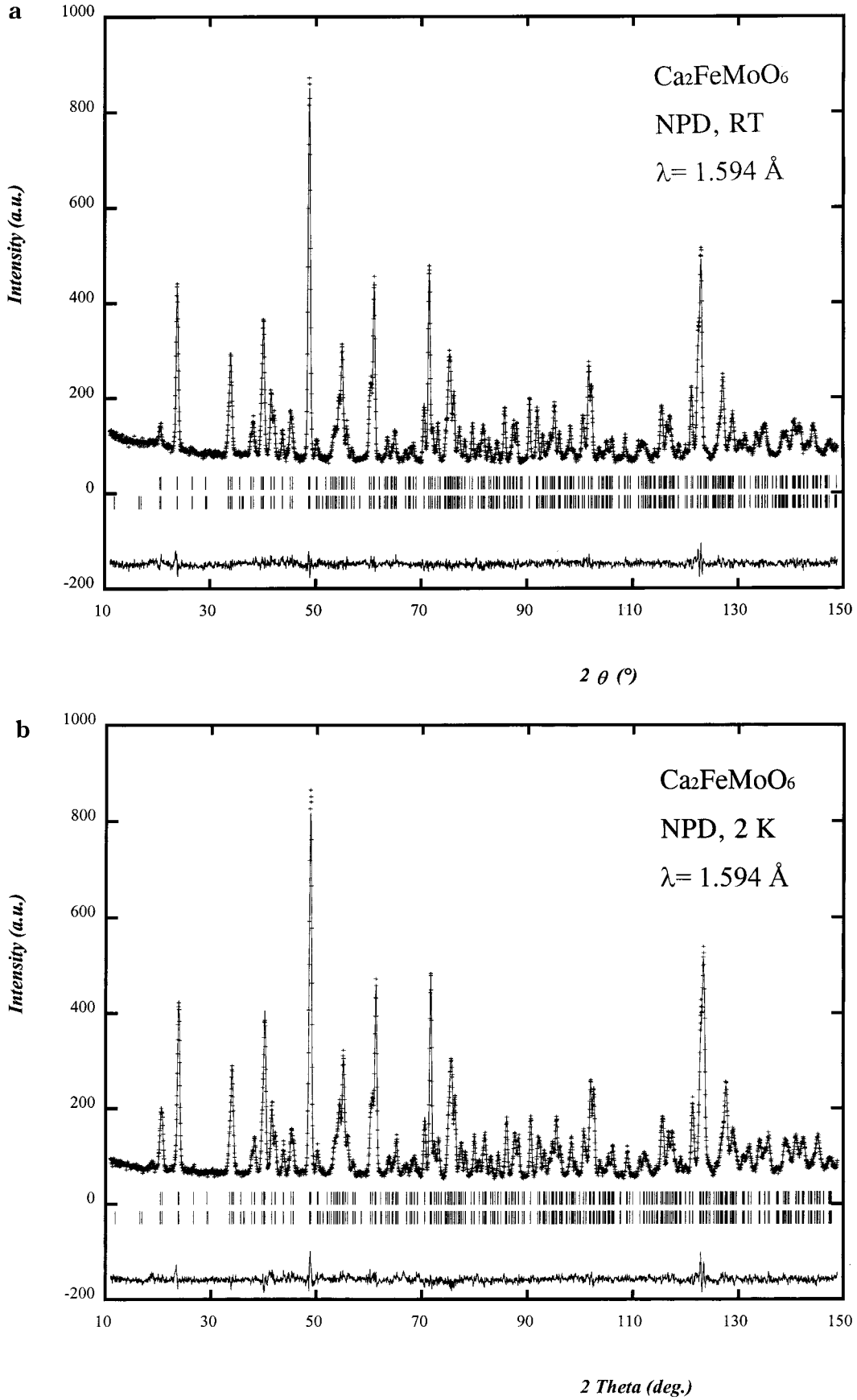

Figure 4. Observed (crosses), calculated (full line) and difference (bottom) NPD Rietveld profiles for Ca_2FeMoO_6 at 295 K and 2 K.

tive to the oxygen positions. A view of the crystal structure of Ca_2FeMoO_6 is shown in Figure 7. It is fairly distorted due to the small size of Ca^{2+} cations, which force the $(Fe,Mo)O_6$ octahedra to tilt in order to optimize the Ca−O bond distances. FeO_6 and MoO_6 octahedra are fully ordered and alternate along the three direc-

Table 1. Unit-Cell, Positional and Thermal Parameters, and Ordered Magnetic Moments for Ca_2FeMoO_6 in the Monoclinic $P2_1/n$ Space Group, $Z = 2$, from NPD Data at 295 and 2 K

	295 K	2 K
a (Å)	5.4150(1)	5.4004(1)
b (Å)	5.5224(1)	5.5219(1)
c (Å)	7.7066(2)	7.6906(2)
β (deg)	89.969(8)	89.971(8)
V (Å^3)	230.455(8)	229.337(9)
	Ca 4e(x y z)	
x	0.9912(7)	0.9920(7)
y	0.0454(3)	0.0474(3)
z	0.251(2)	0.249(2)
B (Å^2)	0.84(4)	0.46(4)
	Fe 2c($^1/_2$ 0 $^1/_2$)	
B (Å^2)	0.54(7)	0.44(8)
magn mom. (μB)	1.7(2)	3.2(1)
	Mo 2d($^1/_2$ 0 0)	
B (Å^2)	0.38(9)	0.01(9)
magn mom. (μB)	−0.5(2)	−0.76(6)
	O1 4e(x y z)	
x	0.0800(4)	0.0814(4)
y	0.4777(4)	0.4770(4)
z	0.2535(12)	0.2539(11)
B (Å^2)	0.74(4)	0.41(3)
	O2 4e(x y z)	
x	0.697(1)	0.6970(9)
y	0.288(1)	0.2859(9)
z	0.041(1)	0.043(1)
B (Å^2)	0.84(13)	0.80(3)
	O3 4e(x y z)	
x	0.210(1)	0.2100(8)
y	0.201(1)	0.1986(8)
z	0.958(1)	0.9560(9)
B (Å^2)	0.56(12)	0.08(3)
	reliability factors	
χ^2	1.35	1.60
R_p (%)	3.77	4.32
R_{wp} (%)	4.76	5.50
R_I (%)	3.89	4.41
R_{mag} (%)	8.88	4.06

tions of the crystal, in such a way that each FeO_6 octahedra is linked to six MoO_6 octahedra, as shown in Figure 7, and vice-versa.

Several examples of monoclinically distorted perovskites have been described in the past, for instance Nd_2MgTiO_6,[16] Ca_2CaUO_6,[17] Sr_2CaUO_6, and Ba_2SrUO_6.[18] In all the cases the compounds crystallize in the $P2_1/n$ space group, with $a \approx b \approx \sqrt{2}a_0$ and $c \approx 2a_0$, and they show long range ordering between the two different cations placed at the B positions of the $A_2B'B''O_6$ perovskite structure. The driving force for the B′, B″ ordering is the charge difference between both kinds of cations, for instance Mg^{2+} and Ti^{4+} in Nd_2MgTiO_6 or Ca^{2+} and U^{6+} in Ca_2CaUO_6. It is remarkable that all of these compounds show an extraordinarily high pseudo-orthorhombic character as far as unit-cell dimensions are concerned: β angles are very close to 90°, for example $\beta = 90.010(9)°$ for Nd_2MgTiO_6.[15] However, the internal symmetry is monoclinic, as shown from neutron diffraction refinements.[16−18] This is also the case for Ca_2FeMoO_6: it is also strongly pseudo-orthorhombic but shows a good and unique convergence in the $P2_1/n$ setting during the refinement of NPD data. As observed

Table 2. Main Bond Distances (Å) and Selected Angles (deg) for Monoclinic Ca_2FeMoO_6 Determined from NPD Data at 295 and 2 K

	295 K	2 K
	FeO_6 Octahedra	
Fe−O1 (×2)	2.005(9)	2.006(8)
Fe−O2 (×2)	2.037(6)	2.045(5)
Fe−O3 (×2)	2.035(6)	2.042(5)
⟨Fe−O⟩	2.026(3)	2.042(5)
	MoO_6 Octahedra	
Mo−O1 (×2)	1.953(9)	1.947(8)
Mo−O2 (×2)	1.944(6)	1.932(5)
Mo−O3 (×2)	1.947(6)	1.942(5)
⟨Mo−O⟩	1.948(3)	1.940(3)
Fe−O1−Mo (×2)	153.6(3)	153.2(3)
Fe−O2−Mo (×2)	152.4(2)	152.4(2)
Fe−O2−Mo (×2)	152.4(2)	151.6(2)
	CaO_9 Polyhedra	
Ca−O1	2.436(3)	2.421(3)
Ca−O1[a]	3.116(4)	3.121(4)
Ca−O1	2.352(4)	2.337(4)
Ca−O2	2.636(11)	2.606(11)
Ca−O2	2.369(12)	2.387(11)
Ca−O2	2.663(14)	2.680(13)
Ca−O2	2.694(14)	2.674(13)
Ca−O3	2.610(14)	2.612(10)
Ca−O3	2.373(12)	2.349(11)
$\langle Ca-O \rangle_{8\ short}$	2.516(4)	2.508(4)
⟨Ca−O⟩	2.583(4)	2.576(4)

[a] Long Ca−O distances.

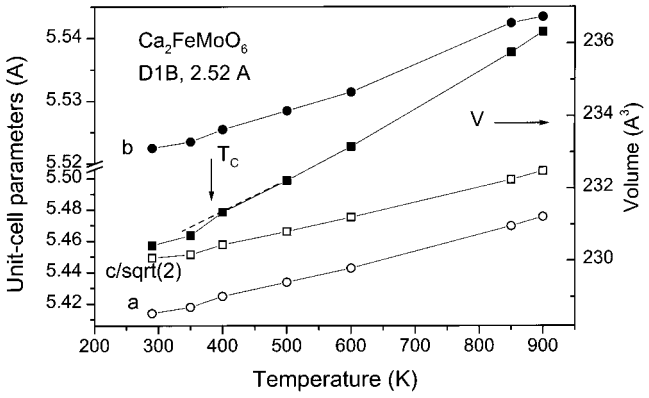

Figure 5. Thermal variation of the lattice parameters and volume from medium-resolution NPD data.

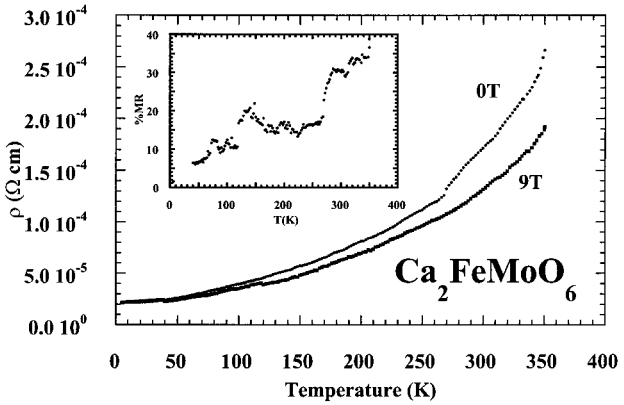

Figure 6. Resistivity versus temperature curves at $H = 0$ and $9T$. The inset shows the thermal variation of magnetoresistance (MR) at $H = 9T$. MR = $100[R(0) - R(9T)]/R(9T)$.

(16) Groen, W. A.; Van Berkel, F. P. F.; IJdo, D. J. W. *Acta Crystallogr. C* **1986**, *42*, 1472.
(17) Van Duivenboden, H. C.; Idjo, D. J. W. *Acta Crystallogr. C* **1986**, *42*, 523.
(18) Groen, W. A.; Idjo, D. J. W. *Acta Crystallogr. C* **1987**, *43*, 1033.

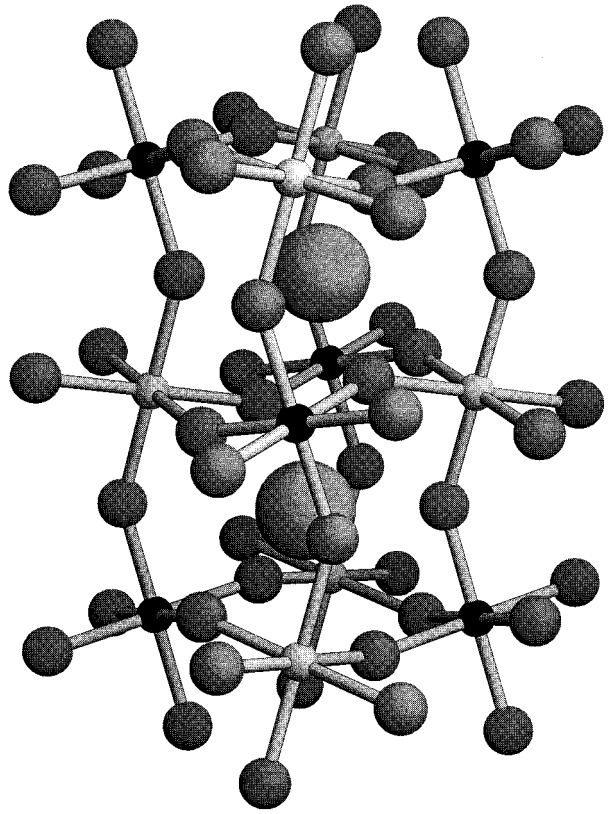

Figure 7. View of the structure of monoclinic Ca_2FeMoO_6. The *c* axis is vertical; the *a* axis is from right to left. Large spheres represent Ca; corner-sharing FeO_6 (dark) and MoO_6 octahedra are fairly tilted in the structure to optimize Ca−O bond lengths.

for Nd_2MgTiO_6, in Ca_2FeMoO_6 the driving force for the monoclinic distortion leading to two independent B positions (Fe and Mo) is also the ordering between two differently charged cations.

As shown in Table 2, FeO_6 octahedra are significantly larger (expanded) than MoO_6 octahedra. This observation is coherent with the larger ionic size of Fe^{3+} versus Mo^{5+}. The average B−O bond lengths at RT compare well with the expected values calculated as ionic radii sums:[19] ⟨Fe−O⟩, 2.026(3) Å (calc 2.025 Å); ⟨Mo−O⟩, 1.948(3) Å (calc 1.99 Å). Moreover, the calculation of the valence of the cations present in the solid is enlightening: the phenomenological Brown's bond-valence model[20] relates the bond length r_i and the valence s_i of a bond (for each central atom $v = \sum s_i$, $s_i = \exp[(r_0 - r_i)/B]$; $B = 0.37$; $r_0 = 1.967$, 1.759, and 1.907 for the Ca−O, Fe−O, and Mo−O pairs).[21] Using this approach, the calculated valences in the ionic limit, from the RT data, are 1.94(2), 2.92(2), and 5.37(4) for Ca, Fe, and Mo cations, respectively. These values suggest that, from the structural parameters, Fe and Mo cations seem to be close to the trivalent and pentavalent oxidation states, although a certain level of mixed valence with Fe^{2+} and Mo^{6+} should not be discarded. It is worth noting the small but significant increase in the average Fe−O distances at 2 K, which could indicate a slight shift of the carrier distribution toward the Fe positions, implying a reduction in the Fe valence at low temperatures.

The actual electronic configurations $Fe^{3+}(3d^5)-Mo^{5+}(4d^1)$ versus $Fe^{2+}(3d^4)-Mo^{6+}(4d^0)$ have been controversial in the cubic perovskite Sr_2FeMoO_6; the Fe^{3+} configuration was considered more probable from Mössbauer spectroscopy studies,[22] but recent low-temperature NPD data[8] support the $Fe^{2+}-Mo^{6+}$ configuration, since a null magnetic moment was observed on the Mo sites ($\mu_{Mo} = 0 \pm 0.1\mu_B$). In contrast, in Ca_2FeMoO_6 we find a small but significant ordered magnetic moment on the Mo sites ($\mu_{Mo} = 0.76 \pm 0.06\ \mu_B$ at 2 K), antiferromagnetically coupled with the Fe magnetic moments in a ferrimagnetic configuration, which is again clearly consistent with the pentavalent oxidation state for Mo. To be noted is the excellent agreement found between the saturation magnetization at 2 K, of 2.5 μ_B per formula unit (Figure 3b), and the net ferrimagnetic moment determined by NPD at 2 K, of 2.4(1) μ_B/f.u., as well as the corresponding values found at 290 K, of 1.1 μB (magnetization) and 1.2(2) μ_B (NPD data) per formula unit.

The ordered magnetic moment found from NPD data at Fe positions, of 3.2(1) μ_B at 2 K, suggests that 3d Fe electrons are in a high-spin configuration. However, the observed value is significantly lower than the expected saturation moment of 5 μB for Fe^{3+} or even of 4μB for Fe^{2+}, which could reflect covalency from the strong Fe−O−Mo superexchange interaction. If we assume that the band structure of this material shows overall features similar to those determined[7,10] for Sr_2FeMoO_6 and Sr_2FeReO_6, we note that there exists density of states at the Fermi level (E_F) only in the down-state band and no state in the up-spin band. The occupied up-spin band below E_F mainly consists of Fe 3d electrons forming the localized spins on the Fe sites, in bands of e_g nature. On the contrary, the down-spin band around E_F is mainly occupied by hybridized Mo 4d t_{2g} and Fe 3d t_{2g} states. We can conclude that the observed value for μ_{Fe} (about 3μB) comes from the two up-spin e_g Fe electrons, which are completely localized at the 2c sites of the perovskite, and the local contribution of a fraction ($\sim 1/3$) of the three electrons occupying bands resulting from the strong overlapping between Mo and Fe t_{2g} and O 2p orbitals, via Fe−O−Mo bonds. This model implies the delocalization of two electrons, giving no (or very small) contribution to the magnetic moment at Fe sites. It is remarkable that the electronic delocalization seems stronger in Ca_2FeMoO_6 than in the Sr analogue, as far as the magnetic localization and the electrical properties are concerned: this situation is against the expected general rule usually fulfilled for perovskite-type compounds, where a stronger structural distortion accounts for a lower orbital overlapping and bandwidth. The conduction mechanism is related to holes (as measured by the Hall effect). Compared with other materials showing colossal magnetoresistance, the observed carrier concentration, of 0.031 per formula unit, is much smaller than that of $La_{2/3}Ca_{1/3}MnO_3$, of 0.18 holes/f.u., but significally higher than that measured in $Tl_2Mn_2O_7$ $\approx$ 0.003 electrons/f.u.[23]

(19) Shannon, R. D. *Acta Crystallogr. A*, **1976**, *32*, 751.
(20) Brown, I. D. In *Structure and Bonding in Crystals*; O'Keefe, M., Navrotsky, A., Eds.; Academic Press: New York, 1981; Vol. 2, pp 1−30.
(21) Brese, N. E.; O'Keefe, M. *Acta Crystallogr. B* **1991**, *47*, 192.
(22) Sleight, A. W.; Weicher, J. F. *J. Phys. Chem. Solids* **1972**, *33*, 679.
(23) Shimakawa, Y.; Kubo, Y.; Manako, T. *Nature* **1996**, *379*, 53.

The microscopic origin of the second anomaly at $T \approx 795$ K could not be determined from the present NPD data, given the smallness of the involved magnetic moments (about 0.07 μ_B/f.u. at 700 K, from magnetization results). We speculate that this small magnetization is coming from Fe_3O_4 or from nanometric and amorphous Fe (or FeMo alloy) particles produced in the surface of the microcrystals during the reduction process. If we assume a value for the saturation magnetization of pure iron (217.5 emu/g at RT), the observed saturation magnetization at 500 K will be related to 0.6−0.7% of pure Fe. This amount of impurity is very difficult to be observed by diffraction methods (or even impossible if the particles are amorphous).

The thermal variation of the unit-cell parameters and volume, shown in Figure 5, displays a significant inflection between 350 and 400 K in *a*, *b*, *c*, and *V*, characterized by an additional contraction when cooling. This effect is clearly associated with the onset of magnetic ordering at $T_C = 380$ K, revealing a coupling between lattice and magnetism. In contrast with the results found for Sr_2FeMoO_6 from thermal expansion measurements, indicating the lack of invar effect in these compounds,[8] our results indeed suggest that there is a change in the electronic itinerancy coupled with the magnetic transition. The contraction of the lattice observed below T_C points out an extra contribution to the chemical bond coming from electronic delocalization as the sample becomes ferromagnetic (ferrimagnetic). This effect is similar to that found in manganese perovskites at the onset of electronic delocalization, coupled with the ferromagnetic ordering via double exchange. The magnitude of this effect is comparable in Ca_2FeMoO_6 ($\Delta V/V = 0.08\%$) and in manganites (e.g. $\Delta V/V = 0.13\%$ for $La_{0.8}Ca_{0.2}MnO_3$[3]); therefore, its presence suggests a similar subjacent mechanism relating metallic behavior and ferromagnetism, which requires further confirmation.

Conclusions

We have shown that Ca_2FeMoO_6 can be prepared as an homogeneous polycrystalline phase from citrate precursors, decomposed, and reduced under an H_2/N_2 flow for a short period of time. A high-resolution NPD study shows that this material is monoclinic, with a strong pseudo-orthorhombic character, and contains Fe^{3+} and Mo^{5+} cations, 1:1 ordered in the B sublattice of the perovskite structure. Below $T_C = 380$ K this phase is ferrimagnetic, showing opposite magnetic moment directions for Fe^{3+} and Mo^{5+}. The low resistivity of this material, as well as the low magnetic moment observed at Fe^{3+} positions, from both magnetization and NPD data, suggests a large delocalization for down-spin Fe^{3+} t_{2g} electrons, even higher than that observed for the Sr and Ba perovskite analogues. The thermal variation of the unit-cell parameters suggests the presence of a significant coupling between spin and lattice, as observed in CMR manganese perovskites.

Acknowledgment. We acknowledge the financial support of CICyT for projects PB97-1181 and MAT97-345, and we are grateful to ILL for making all facilities available.

CM990512G